Symmetry breaking in ionization wave turbulence

S. Niedner and H.-G. Schuster
Institut für Theoretische Physik und Astrophysik, Christian-Albrechts-Universität, D-24098 Kiel, Germany

T. Klinger
Institut für Experimentelle und Angewandte Physik, Christian-Albrechts-Universität, D-24098 Kiel, Germany

G. Bonhomme
Laboratoire de Physique des Millieux Ionisés, Université Henri Poincaré, F-54506 Vandœuvre-lès-Nancy, France
(Received 23 March 1998; revised manuscript received 27 July 1998)

Experimental data of weakly turbulent ionization waves in a plasma glow discharge (a reaction-diffusion system) are analyzed by biorthogonal decomposition. The spatiotemporal dynamics of a single traveling wave and of turbulence are considered. A biorthogonal decomposition analysis of the symmetry properties suggests that turbulence is established here by strong modulation of traveling waves. To mimic this essential feature of the turbulent dynamics, the plasma discharge is periodically perturbed, and a monochromatic traveling ionization wave is modulated in a controlled way. The low-dimensional projection of the spatiotemporal data allows for a reconstruction of the modulation function. Similarities between the periodically perturbed and the turbulent state support the assumption that ionization wave turbulence consists of modulated traveling waves. [S1063-651X(98)06212-6]

PACS number(s): 05.70.Ln, 05.45.−a, 52.35.Ra

I. INTRODUCTION

Probably one of the most challenging subjects in the field of nonlinear dynamical systems is the turbulence problem. Though it has long been investigated, the present situation in the conceptual and theoretical understanding is far from being satisfactory. It has been realized that turbulence is not a unity, i.e., its nature can considerably differ depending on the specific physical system. Prominent examples are the chemical waves (phase turbulence) [1] and neutral fluids [2].

In the present paper, the spatiotemporal dynamics of regular and turbulent plasma ionization waves is studied. Generally speaking, ionization waves are of reaction-diffusion type and are described by a set of partial differential equations of the form

$$\frac{\partial n}{\partial t} = D\Delta n + S(x,t), \tag{1}$$

where the space and time evolution of the density $n(x,t)$ is given by diffusion (with diffusion constant D) and reaction described by the source term $S(x,t)$. Much attention was devoted to chemical waves that develop a particular type of phase turbulence [3]. An often overseen physical system whose collective dynamics is governed by the balance between particle loss and production is the positive column of plasma glow discharges where instabilities in the ionization degree lead to propagating waves, the so-called ionization waves. In Sec. II we give a brief introduction into the physics of ionization waves.

In an empirical approach, grounded on the analysis of experimental observations, we investigate the modulation of spatiotemporal structures and symmetry breaking of regular and turbulent ionization waves. A powerful framework for the study of space-time data is biorthogonal decomposition (BD) [4,5], also known as proper orthogonal decomposition or Karhunen-Loève decomposition [6]. BD provides instruments that are highly sensitive in detecting spatiotemporal symmetries [7] and modulations [8]. Furthermore, BD allows one to identify the energetically most dominant ''modes'' in the spatiotemporal data. These eigenmodes are used as a basis for projection on low-dimensional subspaces considered for further analysis. In a previous study, this general approach gave valuable insights into the bifurcation structure [9] and three-wave coupling [10] of plasma drift waves. Drift waves are based on a Rayleigh-Taylor-type fluid instability, and consequently the turbulence cannot be compared to ionization wave turbulence. Nevertheless, the successful application of the BD formalism in drift wave dynamics encourages one to go here along the same lines. We will come back to this point below.

The paper is organized as follows. In Sec. II, after some notes on the physics of ionization waves, we describe the setup of the plasma experiment. In Sec. III the concepts of BD are summarized. The analysis of the experimental data is done in Sec. IV. We discuss our findings in Sec. V, and make a summary in Sec. VI.

II. EXPERIMENT

The experimental arrangement consists of a cold-cathode discharge tube (length $L=50$ cm, diameter $d=3.0$ cm) that is operated with neon as neutral gas (pressure $p=1-2$ mbar). The discharge is sustained by an externally applied voltage and the current ($I_d=10-20$ mA) is limited by a series resistor (Fig. 1). The integral light flux is picked up by a linear array of 64 phototransistors, positioned along the homogenous positive column of length $l=40$ cm. In this way the fluctuations of the light flux are simultaneously recorded in space and time. The distance between each two

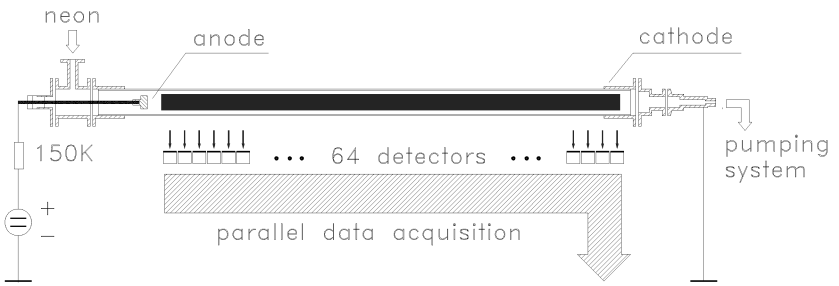

FIG. 1. Schemtic diagram of the experimental device. The (spectrally) integral light emission is recorded by a linear array of 64 photodetectors.

photo transistors is $\Delta x = l/63 = 0.635$ cm and the sampling rate is $\Delta t = 30\ \mu$s with eight-bit accuracy. The resulting Nyquist limits are $k_{\mathrm{Ny}} = 0.79\ \mathrm{cm}^{-1}$ and $f_{\mathrm{Ny}} = 16.6$ kHz, respectively.

It is known that in a certain range of operation the light flux fluctuations are caused by moving striations, also known as ionization waves [11]. In general, ionization waves are axially propagating in the positive column of glow discharge plasmas operated at a base pressure of a few mbar, where the ionization degree is low and the particle motion is dominated by diffusion in the externally applied electric field. Reviews on the physical properties of the positive column and earlier investigations on ionization waves can be found in Refs. [11–13]. It was discovered that ionization waves are essentially one-dimensional phenomena since the diffusion in the radial direction (we restrict the discussion to cylindrical geometry) can be approximated by the particle lifetime only. Roughly speaking, ionization waves are temperature waves leading to propagating fluctuations in the ionization degree. The latter establishes density fluctuations $n(x,t)$ propagating axially as traveling waves. The source term in Eq. (1) is then given by $S(x,t) = I(x,t) - R(x,t)$, where $I(x,t)$ is the ionization (particle production) and $R(x,t)$ is the recombination (particle loss) due to wall losses. The dynamics $\partial_t n$ of ionization waves is determined by the balance between the source term $S(x,t)$ and the axial diffusion term.

The linear dynamics of ionization waves is reasonably well understood [13,14]. On the other hand, ionization wave turbulence, despite valuable experimental observations and modeling attempts [15,16], still bears many open questions. We emphasize that many of these questions (for instance the formation and dynamics of spatiotemporal patterns) are of quite general nature and are not seen as being specific for ionization waves. Recent investigations have focused on the temporal ionization wave chaos emerging in autonomous [17] and nonautonomous discharges [18–20]. In the autonomous case, the chaos establishes spontaneously in certain parameter regimes. In contrast, the ionization wave chaos in the nonautonomous case is excited by an externally applied driving force, i.e., a weak modulation (typically $<5\%$) of the discharge current. In this kind of discharge experiment, the methods of ''controlling chaos'' [21] have recently been applied with some success [22–24].

III. BIORTHOGONAL DECOMPOSITION

For the biorthogonal decomposition of two-dimensional spatiotemporal data $u(x,t) \in X \times T$ where $X = [0,L]$ and $T = [t_0, t_1]$ we define two operators on the Hilbert spaces $H(X)$ and $H(T)$:

$$U\phi(x) = \int_X u(x,t)\,\phi(x)\,dx, \tag{2}$$

$$U^\dagger \psi(t) = \int_T u(x,t)\,\psi(t)\,dt. \tag{3}$$

The operators U and $U^\dagger$ map $H(X)$ into $H(T)$, and vice versa. In our calculations, we use the L^2 norm. Assuming compactness of U one obtains a discrete spectrum of U and $U^\dagger$ [4]. The corresponding eigenvalue problems

$$U\phi_k(x) = \alpha_k \psi_k(t)\,, \tag{4}$$

$$U^\dagger \psi_k(t) = \alpha_k \phi_k(x) \tag{5}$$

are closely related to the eigenvalue problem for the autocorrelation function [5]:

$$UU^\dagger \psi_k(t) = \int_X \int_T u(x,t)u(x,t')\,\psi_k(t)\,dx\,dt' = \alpha_k^2 \psi_k(t). \tag{6}$$

This allows for a decomposition of $u(x,t)$ in the form

$$u(x,t) = \sum_{k=1}^{\infty} \alpha_k \phi_k(x)\,\psi_k(t). \tag{7}$$

The functions $\phi_k(x)$ and the $\psi_k(t)$ (called *topos* and *chronos*, respectively) are orthonormal, i.e., $(\phi_k, \phi_j) = (\psi_k, \psi_j) = \delta_{k,j}$. The *weights* α_k are real numbers, arranged such that $\alpha_k \geqslant \alpha_l$ for $k > l$. Their distribution is quantified by the BD energy E and BD entropy H that are defined by

$$E = \int_X \int_T u(x,t)u^*(x,t)\,dx\,dt = \sum_{k=1}^{\infty} \alpha_k^2, \tag{8}$$

$$H = \lim_{N\to\infty} -\frac{1}{N} \sum_{k=1}^{N} p_k \ln p_k \tag{9}$$

with $p_k = \alpha_k^2/E \in [0,1]$. For the analysis of phase evolutions it was introduced in Ref. [9] the *complexification* of a pair (j,k) of topos and chronos:

$$\begin{aligned} \Phi_{(j,k)}(x) &= \phi_j(x) + i\,\phi_k(x), \\ \Psi_{(j,k)}(t) &= \psi_j(t) + i\,\psi_k(t). \end{aligned} \tag{10}$$

As already shown in Refs. [9,10] the phase portrait of $\Phi_{(j,k)}(t)$ (polar plot) reveals the temporal periodicity of the wave. The complexification yields a *frequency*

$$\nu_{(j,k)}=\frac{d}{dt}\arg\Psi_{(j,k)}(t) \tag{11}$$

for the reconstructed BD structure. Analogously, a *wave number* $\kappa_{(j,k)}$ is defined for the corresponding topos. The reconstruction $\Xi_{(j,k)}(x,t)$ of a BD structure corresponding to a specifically chosen BD weight pair (α_j,α_k) is given by

$$\Xi_{(j,k)}(x,t)=\alpha_j\phi_j(x)\psi_j(t)+\alpha_k\phi_k(x)\psi_k(t). \tag{12}$$

This reconstruction is a particular two-dimensional subspace of the typically high-dimensional original system.

The observed data (discrete in time and space) is written as a matrix $u_{i,j}=u(x_i,t_j)$. The BD then becomes equivalent to the singular value decomposition of the matrix u. The chronos and topos are then the respective eigenvectors of the temporal and the spatial autocorrelation matrix. It was pointed out in Ref. [25] that the lack of scaling invariance can be circumvented by normalizing each time series to its standard deviation σ^2 after subtracting its average value. Following this approach, the experimental data are normalized as follows:

$$u'_{i,j}=\frac{1}{\sigma_i^2}\left(u_{i,j}-\sum_j u_{i,j}\right). \tag{13}$$

For simplicity, we further drop the prime. The implied assumption of temporal homogeneity is justified for the present case. We note that Eq. (13) is equivalent to a normalization with respect to the global energy E.

There are two features that make the BD superior to other decompositions, its optimality and its ability to detect spatiotemporal symmetries. It has been shown [6] that among all linear decompositions, the BD is the most efficient for modelling or reconstructing a signal $u(x,t)$, in the sense of capturing the most kinetic energy possible for a projection on a given number of modes. Of special interest in the present study is spatiotemporal symmetry, in particular uniformly traveling waves (UTW's). They are of the general form

$$u(x,t+t_0)=u(x-x_0,t), \tag{14}$$

where $c=x_0/t_0$ is the propagation velocity. This leads to a multiplicity of the BD weights, and the BD is equivalent to a Fourier decomposition [7].

More complex spatiotemporal structures linked to degenerated BD weights are *modulated* uniformly travelling waves (MUTW's) [8]. They are defined by their two modulation functions $M(x):X\rightarrow\mathbb{R}$ and $N(t):T\rightarrow\mathbb{R}$

$$\tilde{\Xi}(x,t)=M(x)N(t)[\alpha_j\phi_j(x)\psi_j(t)+\alpha_k\phi_k(x)\phi_k(t)], \tag{15}$$

where $\psi_j(t),\psi_k(t)$ and $\phi_j(x),\phi_k(x)$ are given by the biorthogonal decomposition of a UTW. The corresponding complexifications (10) read

$$\tilde{\Phi}_{(j,k)}(x)=M(x)\Phi_{(j,k)}(x), \tag{16}$$

$$\tilde{\Psi}_{(j,k)}(t)=N(t)\Psi_{(j,k)}(t).$$

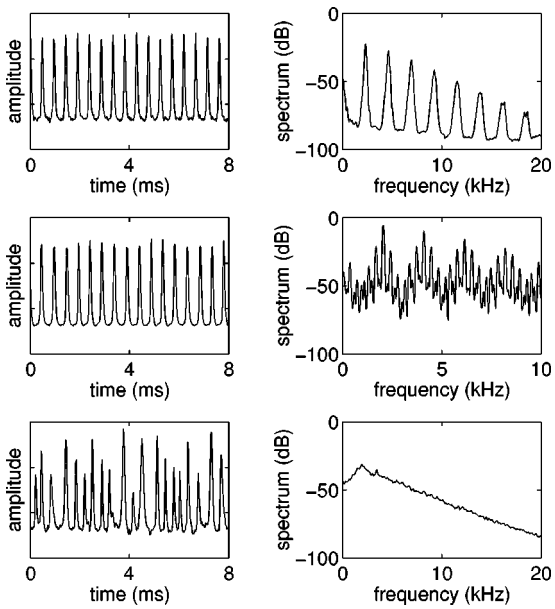

FIG. 2. Time traces and power spectra of the light fluctuations taken from a single, arbitrarily chosen, photodetector. The three observed dynamical states are (a) regular, (b) quasiperiodic, and (c) turbulent. The quasiperiodic state (b) is observed in the nonautonomous discharge with a periodic driver of frequency $f_d=1.68$ kHz.

The structure of the topos and chronos of the MUTW allows one to specify the form of $M(x)$ and $N(t)$. Since the topos and chronos are no longer simple Fourier modes, conventional spectral analysis cannot accomplish this task [7].

IV. RESULTS

Three different dynamical states of ionization waves are considered for the BD analysis. As mentioned above, the autonomous discharge experiment is typically found either in a regular state (a single ionization wave) or in the turbulent state, depending on the set of operation parameters, i.e., neutral gas pressure and discharge current. These two generic states are studied in Sec. IV A. To develop a better understanding of the complex dynamics in the observed turbulence, we additionally consider a quasiperiodic state that is established in the discharge by a periodic external perturbation (Sec. IV B). This allows for a detailed investigation of the properties of MUTW's which are shown to play an important role in the present kind of turbulence. The validity of the chosen approach is supported by the fact that the transition to turbulence in the periodically driven (nonautonomous) discharge follows the quasiperiodicity route [19]. Ionization wave turbulence in the autonomous and in the nonautonomous discharge system has very similar dynamical properties.

Figure 2 shows time series of the light emission and the corresponding power spectra of the three different dynamical states. The regular state is characterized by a periodic oscillation of the light emission. The power spectrum is sharply peaked at $f_0=2.31$ kHz, with pronounced higher harmonics due to the nonsinusoidal shape of the fluctuations. In the quasiperiodic state, the nonlinear interaction between the self-excited ionization wave (with frequency $f_0=2.06$ kHz

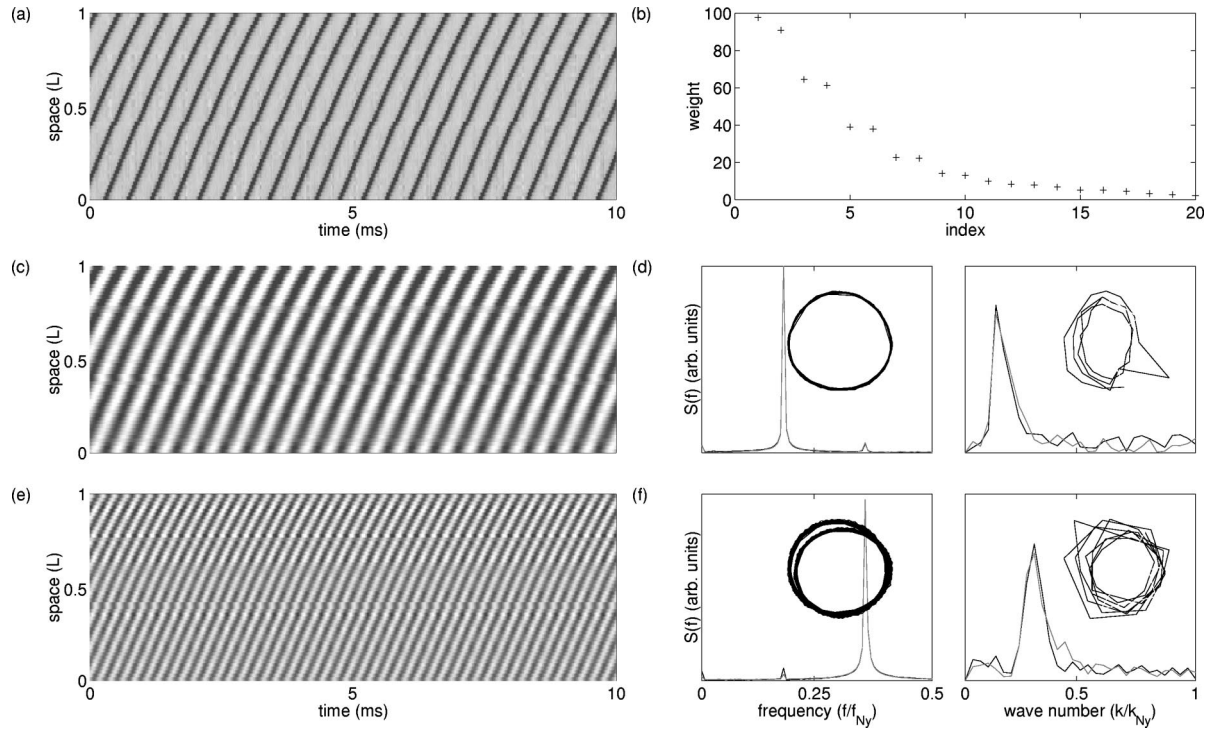

FIG. 3. BD analysis of the regular state. (a) Spatiotemporal raw data. (b) Distribution of the most important BD weights. (c) Reconstruction $\Xi_{(1,2)}(x,t)$. (d) Fourier spectra of chronos $\psi_1(t)$ and $\psi_2(t)$ with their complexification shown in the inset (left), and Fourier spectra of topos $\phi_1(x)$ and $\phi_2(x)$ with their complexification shown in the inset (right; the first and the last six points of each complexification have been shaded gray to demonstrate finite size effects). (e) Reconstruction $\Xi_{(3,4)}(x,t)$. (f) Same as (d) for pair (3) and (4).

and higher harmonics) and the driver (with frequency $f_d = 1.68$ kHz and higher harmonics) leads to the occurrence of sidebands at frequencies $f = nf_0 \pm mf_d$ $(n,m \in \mathbb{N})$. In the turbulent state, the time series is strongly irregular, especially in the phase, and the power spectrum is broad. We find a close similarity of the shape of the fluctuation signals to certain solutions of the Kuramoto-Sivashinsky equation [5,26].

For the subsequent discussion of the BD analysis of the experimental data, we have chosen the following common layout. Each dynamical state is described by a group of diagrams. In the first row, we show the normalized spatiotemporal data and the spectrum of BD weights. The second and third rows show selected pairs of chronos and topos, i.e., the reconstruction $\Xi_{(j,k)}(x,t)$ [cf. Eq. (12)] and the Fourier spectra (linear scale) of the chronos and topos pairs (j,k). The phase portrait of the complexification (10) is shown in the insets of the corresponding Fourier spectra. Here and during the subsequent discussion frequencies are expressed in units of the Nyquist frequency.

A. Autonomous system

Figure 3 shows the result of the BD analysis of the regular (time and space periodic) state of the ionization waves. The symmetry condition (14) is clearly satisfied and pairs $\alpha_{2i-1} = \alpha_{2i}$ $(i = 1,2,\ldots)$ of degenerated weights are formed. Each of them corresponds to a traveling wave with the same spatiotemporal symmetry (14), meaning the same phase velocity. The spectra of the chronos are nearly δ-peaks at $f_0 = 0.15$ and $2f_0 = 0.30$. Hence the BD modes are equivalent to Fourier modes, and the subspace $\Xi_{(3,4)}(x,t)$ is simply the first harmonic of subspace $\Xi_{(1,2)}(x,t)$. This finding is consistent with the above statement on the constant phase velocity of the BD modes, a hallmark of higher harmonics. The phase portraits of the complexifications shows the regularity of the chronos and topos. They form nearly perfect circles, which is a further indication of equivalence to Fourier modes, which are the most natural description of UTW's.

The turbulence state of the plasma column is shown in Fig. 4. Here, the degeneracy of the BD weights is much less obvious and, to form pairs, we have to rely on similarities in the Fourier spectra of the chronos and topos. The most energetic reconstruction $\Xi_{(1,2)}(x,t)$ still contains a significant regular part, indicated by the pronounced peak at $f_0 = 0.19$ in the Fourier spectrum. However, in contrast to the regular state (Fig. 3), the spectrum shows additional components at $f < f_0$ with a peak at $f_1 = 0.10$. The BD modes thus strongly deviate from Fourier modes, indicating spatiotemporal modulations. The situation is very similar in the reconstruction $\Xi_{(3,4)}(x,t)$. The phase velocities $\nu_{(1,2)}$ and $\nu_{(3,4)}$ are strongly changing in time, reflecting the varying slope of the wave fronts in the reconstruction. The wave numbers $\kappa_{(1,2)}$ and $\kappa_{(3,4)}$ remain nearly constant in time (not shown). The phase portraits of the chronos and topos of $\Xi_{(1,2)}(x,t)$ and $\Xi_{(3,4)}(x,t)$ are not circular but are almost space filling. Reconstructions $\Xi_{(j,j+1)}(x,t)$ of higher order $j > 4$ have a similar structure and are not shown.

Both the multipeaked power spectra and the noncircular phase portraits of the chronos and topos pairs suggest strong modulation of UTW's. At this point, however, it is difficult to specify the modulation type precisely. In Ref. [9], for a different physical situation (drift waves in magnetized plas-

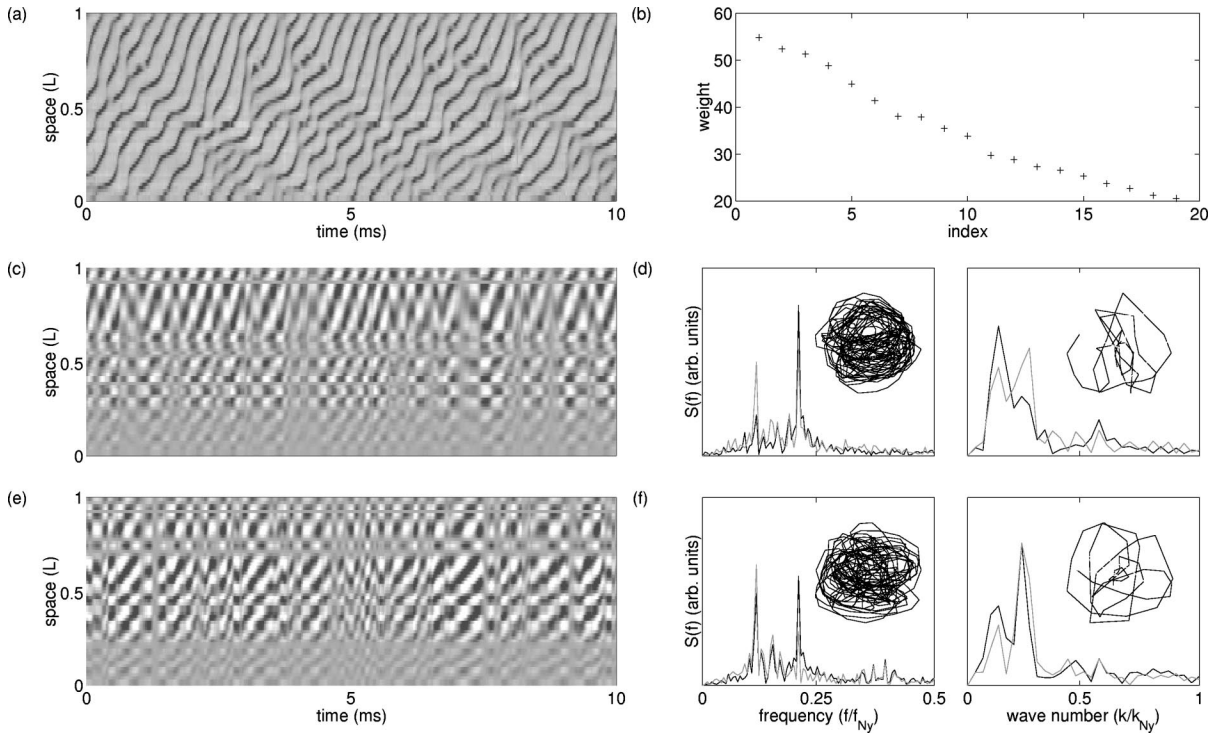

FIG. 4. BD analysis of the turbulence state. (a) Spatiotemporal raw data. (b) Distribution of the most important BD weights. (c) Reconstruction $\Xi_{(1,2)}(x,t)$. (d) Fourier spectra of chronos $\psi_1(t)$ and $\psi_2(t)$ with their complexification shown in the inset (left), and Fourier spectra of topos $\phi_1(x)$ and $\phi_2(x)$ with their complexification shown in the inset (right; the first and the last six points of each complexification have been shaded gray to demonstrate finite size effects). (e) Reconstruction $\Xi_{(3,4)}(x,t)$. (f) Same as (d) for pair (3) and (4).

mas), complex modulation of UTW's was considered. In a recent theoretical study, real-valued modulation functions of type (15) have been investigated in detail. Tentatively, we conclude that ionization wave turbulence is characterized by symmetry modifications due to strong modulation of UTW's. Due to the complicated structure of the two-dimensional reconstructions, the construction of the full set of different modulation functions is a very demanding task. As a first step toward this goal, a highly simplified situation, the quasiperiodic state, is studied in Sec. IV B. Roughly speaking, the quasiperiodic state can be seen as the lowest order approximation to turbulence.

We finally note that the analysis of the turbulent data set is facilitated by the BD approach. The mutual mapping between chronos and topos established by Eq. (5) yields the spatiotemporal reconstructions (12) of BD modes that are clearly more complex than Fourier modes. The reconstructions, discussed together with their weights, provide a more detailed view of the spatiotemporal patterns present in the turbulent system.

B. Nonautonomous system

To investigate more precisely the modulation effect of traveling waves, the discharge is driven externally by a periodic current modulation. This launches a second ionization wave mode with the frequency of the driver signal $f_d = 0.12$. As a result, a quasiperiodic state is established which is considered here as the weakest form of turbulent dynamics.

The spatiotemporal data of the quasiperiodic state is shown in Fig. 5. There is still a pronounced degeneracy in the weights and four BD reconstructions $\Xi_{(j,j+1)}(x,t)$ ($i=1,\ 3,\ 5,$ and 7) are identified. The first reconstruction $\Xi_{(1,2)}(x,t)$ has exactly the same features as the one in the regular state Fig. 3. The BD modes are equivalent to Fourier modes, and are specified as UTW's. The same holds for $\Xi_{(3,4)}(x,t)$ and $\Xi_{(5,6)}(x,t)$ (not shown). The subsystem $\Xi_{(7,8)}(x,t)$, however, represents a modulated UTW: The phase portraits of $\Phi_{(7,8)}(x)$ and $\Psi_{(7,8)}(t)$ show that the phase evolution is varying in time and the Fourier spectrum is multipeaked. To provide an overview, the frequencies and wave numbers in the quasiperiodic state are compiled in Table I.

The first three pairs form a group of higher harmonics, comparable to the regular state described in Sec. IV A. All these frequencies and wave numbers are incommensurate to the most dominant frequency component found in the Fourier spectrum of the chronos pair [Eqs. (7) and (8)]. This is an important feature of the quasiperiodic state, and the dominant frequency component in the spectrum is identified with a second ionization wave, launched by the external periodic perturbation. It was pointed out in Ref. [8] that the spatiotemporal modulation introduces additional sidebands (here at $f_n = 0.124 \pm m\Delta f$ with $\Delta f = 0.023$ and $m \in \mathbb{N}$) in the Fourier spectra of the chronos and topos. The group velocity of the wave is given by $c_g = 2\pi \partial\nu/\partial\kappa$. It is suggested by the values listed in Table I that the group velocity of the wave has a negative sign (the higher frequency mode has a lower wave number). It is indeed one of the most prominent features of ionization waves to be backward waves, i.e., to have phase and group velocities with opposite sign.

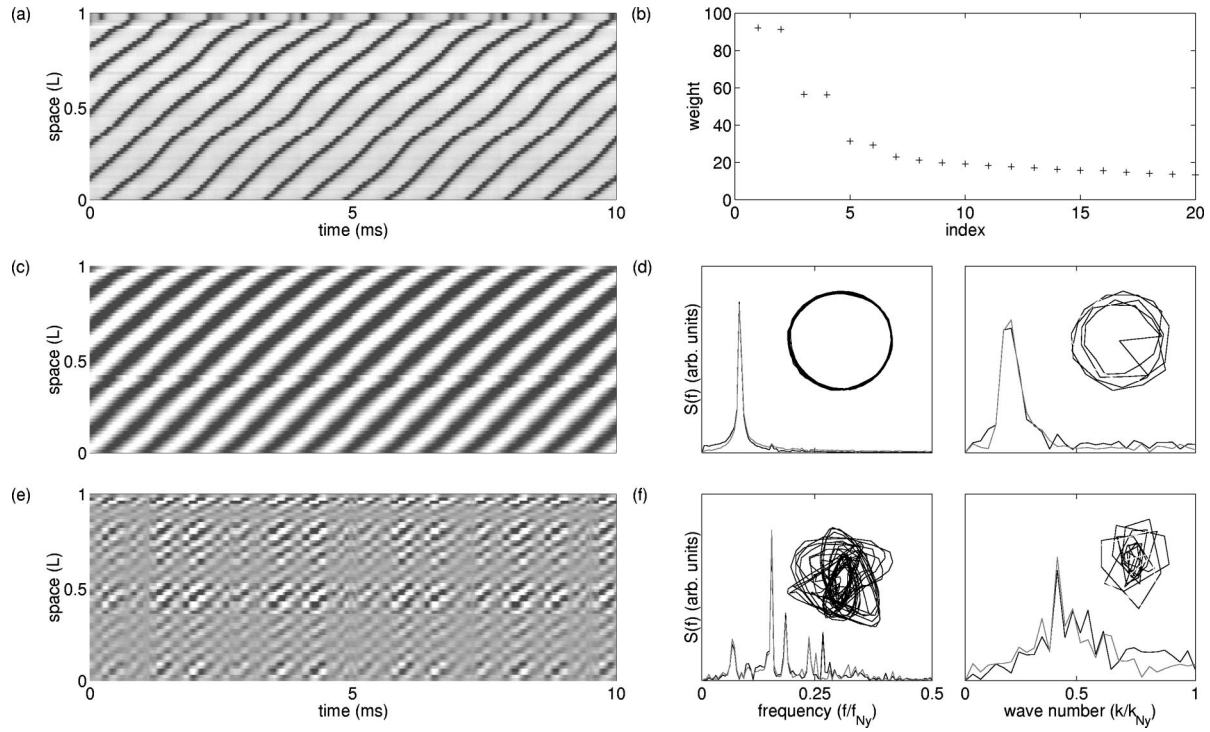

FIG. 5. BD analysis of the quasiperiodic state. (a) Spatiotemporal raw data. (b) Distribution of the most important BD weights. (c) Reconstruction $\Xi_{(1,2)}(x,t)$. (d) Fourier spectra of chronos $\psi_1(t)$ and $\psi_2(t)$ with their complexification shown in the inset (left), and Fourier spectra of topos $\phi_1(x)$ and $\phi_2(x)$ with their complexification shown in the inset (right; the first and the last six points of each complexification have been shaded gray to demonstrate finite size effects). (e) Reconstruction $\Xi_{(7,8)}(x,t)$. (f) Same as (d) for pair (7) and (8).

C. BD entropies

As discussed in Sec. III, the BD entropy provides a reasonable measure of the spatiotemporal complexity of the dynamics. In Table II, the computed values of the BD entropies Eq. (9) are listed for the three different dynamical states. Since in the transition from the regular to the turbulent state the energy is spread over the different BD modes, there is a pronounced raise in the entropy. We bear in mind that the information on the BD energy was already introduced in the normalization (13).

V. DISCUSSION

In the general class of reaction-diffusion systems, ionization waves are seen as a revealing example. This is motivated by the processes involved in the physical ionization wave mechanism. The motion of the charged particles is governed by diffusion, and the particle balance is determined by ionization and recombination losses. To some extent, it is thus reasonable to expect experimental observations in ionization wave turbulence to be of relevance for the nonlinear dynamics of reaction-diffusion systems in general. Consequently, in the present discussion, we focus our attention on universal spatiotemporal structures rather than on the microscopic physical mechanisms involved.

The approach chosen in the present paper is based on the projection of the spatiotemporal dynamics on low-dimensional subspaces spanned by the most energetic eigenmodes of the biorthogonal decomposition, also called ''empirical eigenmodes'' [6] owing to the fact that they are solely determined by the experimental observation. We restrict the discussion to the symmetry properties of the subspaces. It is the main goal of the present study to examine how the symmetry of spatiotemporal structures changes when comparing ionization waves in regular and turbulent states. To achieve this goal, spatiotemporal data for regular, quasiperiodic, and turbulent states are taken into consideration. We note that the quasiperiodic state is generally not observed in the autonomous discharge experiment.

TABLE I. Frequencies, wave numbers, and phase velocities $c_n = f_n/k_n$ of the BD modes in the quasiperiodic state. The frequency uncertainty of the spectral peaks is $\delta f = 0.005$.

(i,j)	f_n	k_n	c_n
(1,2)	0.08	0.07	1.14
(3,4)	0.16	0.14	1.14
(5,6)	0.24	0.21	1.14
(7,8)	0.124	0.407	0.302
	0.188	0.531	0.354
	0.056	0.312	0.179
	0.212	0.641	0.331
	0.148	0.469	0.354

TABLE II. The BD entropy of different dynamical states.

State	Entropy
regular	0.44
quasi-periodic	0.55
turbulent	0.80

The most simple situation is the regular state where only one traveling wave is present. The BD weights are ordered in a sequence of degenerated pairs, each of them corresponding to the same spatiotemporal symmetry (14). This is revealed by the agreement of the phase velocities $c_{(j,j+1)}$ of the different BD reconstructions $\Xi_{(j,j+1)}$. The linear superposition of the reconstructions forms the (nonmonochromatic) uniformly traveling wave. According to Ref. [7], the BD here is fully equivalent to a Fourier analysis.

At first glance, the weight distribution of the quasiperiodic state looks very similar. The BD weights are still ordered in pairs, indicating spatiotemporal symmetry, but the additional wave with the new frequency corresponding to the pair [Eqs. (7) and (8)] introduces a different propagation velocity $c_{(7,8)} \neq c_{(1,2)}$ (cf. Table I) and a new symmetry [8]. The Fourier spectrum of $\Xi_{(7,8)}$ shows pronounced side bands clearly indicating a MUTW [8]. The complexifications (16) of a MUTW with frequency ω, wave number k, and phase velocity $c=\omega/k$ simply read

$$\tilde{\Phi}_{(7,8)}(x) = M(x)\exp(ikx), \tag{17}$$

$$\tilde{\Psi}_{(7,8)}(t) = N(t)\exp(i\omega t). \tag{18}$$

We specify the real-valued modulation functions $M(x)$ and $N(t)$ by the *phase modulation* ansatz

$$M(x) = \tfrac{1}{2}[\exp\{i\mu_x \sin(k'x)\} + \exp\{-i\mu_x \sin(k'x)\}], \tag{19}$$

$$N(t) = \tfrac{1}{2}[\exp\{i\mu_t \sin(\omega' t)\} + \exp\{-i\mu_t \sin(\omega' t)\}]. \tag{20}$$

Since the exponential expressions in Eqs. (19) and (20) are generating functions, they can be expressed in a series expansion

$$\exp[i\mu_x \sin(k'x)] = \sum_{n=-\infty}^{\infty} J_n(\mu_x)\exp(ink'x), \tag{21}$$

where the $J_n(\mu_x)$ are the Bessel functions of order n. Similar expressions are obtained for $N(t)$ and since $J_n(-x) = (-1)^n J_n(x)$ we finally obtain, for the complexifications,

$$\tilde{\Phi}_{(7,8)}(x) = \sum_{n=-\infty}^{\infty} \mu_x^n \exp[i(2nk'+k)x], \tag{22}$$

$$\tilde{\Psi}_{(7,8)}(t) = \sum_{m=-\infty}^{\infty} \mu_t^m \exp[i(2n\omega'+\omega)t], \tag{23}$$

with the new modulation coefficients $\mu_x^n = J_{2n}(\mu_x)$ and $\mu_t^m = J_{2m}(\mu_t)$. The two-dimensional subsystem reads

$$\Xi_{(7,8)}(x,t) = \mathrm{Re}[\tilde{\Phi}_{(7,8)}(x)]\mathrm{Re}[\tilde{\Psi}_{(7,8)}(t)] + \mathrm{Im}[\tilde{\Phi}_{(7,8)}(x)]\mathrm{Im}[\tilde{\Psi}_{(7,8)}(t)] \tag{24}$$

TABLE III. Modulation coefficients of the quasiperiodic state.

$\omega = 0.124$	$k = 0.407$
$\omega' = \Delta\omega/2 = 0.0125$	$k' = \Delta k/2 = 0.036$
$\mu_{-3}^t = 3.129$	
$\mu_{-2}^t = 0$	
$\mu_{-1}^t = 0$	$\mu_{-1}^x = 0.79$
$\mu_0^t = 11.89$	$\mu_0^x = 3.13$
$\mu_1^t = 1.5$	$\mu_1^x = 1.89$
$\mu_2^t = 0$	$\mu_2^x = 1.49$
$\mu_3^t = 3.46$	$\mu_3^x = 1.29$
$\mu_4^t = 2.06$	

Without loss of generality, we set $\alpha_7 = \alpha_8 = 1$. After some manipulations for Eq. (24) we obtain the expression

$$\Xi_{(7,8)}(x,t) = \sum_{n=-\infty}^{\infty}\sum_{m=-\infty}^{\infty} \mu_n^x \mu_m^t \cos[(k+2nk')x + (\omega+2m\omega')t]. \tag{25}$$

This is identical with the formula given in Ref. [8]. The coefficients μ_n^x and μ_m^t and the modulation frequencies ω' and k' can be explicitly estimated by the experimentally obtained Fourier spectra of the chronos and the topos. We find the values given in Table III.

The relatively small μ_n^x and μ_m^t with $|n|>4$ are neglected. We note that phase modulation suppresses sidebands with odd multiples of the modulation frequency ω'. Following the classification of Ref. [8], the Fourier sidebands are *resonant*. The chronos and topos are no longer Fourier modes, meaning that the symmetry relation (14) is no longer valid. The spatiotemporal translation symmetry of the regular state is changed by the spatial and temporal modulation. In Fig. 6 the two-dimensional subsystem (25) is depicted. There are many features of the reconstructed modulation function that agree well with experimental observations. The

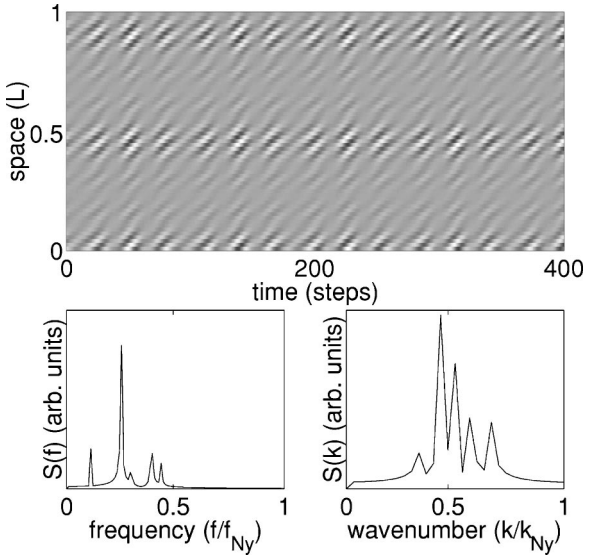

FIG. 6. Model description of the spatiotemporal dynamics of the quasiperiodic state. (a) Spatiotemporal pattern. (b) Fourier spectrum of chronos and topos.

comparison between Fig. 6 and the two-dimensional BD reconstructions (Figs. 5 and 4) shows that the spatially localized amplitude crashes (wave amplitude nearly vanishes) as well as the periodic occurrence of short wave trains are solely caused by phase modulation [Eqs. (19) and (20)]. Both in turbulent and quasiperiodic states, the two-dimensional subsystems of MUTW's have these two features; in the turbulent state the sequence of crashes and wave trains is slightly more complicated. The pronounced time evolution of the wave amplitude is also the reason for the space-filling phase portraits of the topos and chronos in Figs. 5(f), 4(d), and 4(f). The power spectra of the chronos and topos agree by construction. In Ref. [9] plasma drift waves were investigated following essentially the same strategy. The modulation of waves turned out to be a valuable concept as well, but the modulation is complex valued, and consequently the two-dimensional subsystems have a more complicated time evolution.

From the discussion above, we conclude that the turbulence state is established by increasing phase modulation in space and time of the involved waves. The modulation leads to a breaking of the spatiotemporal symmetry. The phase modulation becomes evident by inspection of the Fourier spectra and the phase portraits of chronos and topos in the turbulent state (cf. Fig. 4). The multipeaked spectra and the noncircular phase portraits suggest that a modulation similar to the one observed in the quasiperiodic state occurs. The increase of the BD entropy (cf. Table II) defined by Eq. (9) quantifies the increase of spatiotemporal disorder during the transition to turbulence [27].

VI. SUMMARY

In this paper we investigated symmetry properties of turbulence in a plasma discharge, that is used as an example for a reaction-diffusion system. The analysis is done by biorthogonal decomposition (BD), which is superior to Fourier analysis with respect to the detection of spatiotemporal symmetries. We investigated the role of modulated traveling waves in the development of turbulence and the quasiperiodic state of a nonautonomous (periodically forced) discharge. The analysis of the symmetry properties of the BD eigenmodes reveals the importance of modulated uniformly traveling waves. Modulation leads to a breaking of spatiotemporal symmetries. Suggested by the experimental observation, phase modulation was assumed to be the predominant process. From the BD analysis the modulation function was explicitly reconstructed, and a good agreement with the experimental results was found.

ACKNOWLEDGMENTS

We gratefully acknowledge fruitful discussions with Dr. T. Dudok de Wit and Dr. Ricardo Lima. Dr. Anatol Atipo is gratefully thanked for his stimulating suggestions during the early stage of the present work.

[1] M. C. Cross and P. C. Hohenberg, Rev. Mod. Phys. **65**, 851 (1993).
[2] U. Frisch, *Turbulence* (Cambridge University Press, Cambridge, 1995).
[3] P. Foerster, S. C. Müller, and B. Hess, Science **241**, 685 (1988).
[4] N. Aubry, R. Guyonnet, and R. Lima, J. Stat. Phys. **64**, 683 (1991).
[5] N. Aubry, R. Guyonnet, and R. Lima, J. Nonlinear Sci. **2**, 183 (1992).
[6] P. J. Holmes, J. L. Lumley, G. Berkooz, J. C. Mattingly, and R. W. Wittenberg, Phys. Rep. **287**, 337 (1997).
[7] N. Aubry, F. Carbone, R. Lima, and S. Slimani, J. Stat. Phys. **76** (1994).
[8] N. Aubry and R. Lima, Chaos **5**, 578 (1995).
[9] A. Madon and T. Klinger, Physica D **91**, 301 (1996).
[10] A. Madon and T. Klinger, Physica D **102**, 335 (1997).
[11] N. L. Oleson and A. W. Cooper, Adv. Electron. Electron Phys. **24**, 155 (1968).
[12] L. Pekárek and J. Krása, in *Proceedings of the Yugoslav Symposium and Summer School on the Physics of Ionized Gases, Invited Lectures*, edited by V. Vujnović (Institute of Physics of the University of Zagreb, Rovinj, Yugoslavia, 1974), pp. 915–952.
[13] R. N. Franklin, *Plasma Phenomena in Gas Discharges*, The Oxford Engineering Science Series (Clarendon, Oxford, 1976).
[14] Y. P. Raizer, *Gas Discharge Physics* (Springer, Berlin, 1991).
[15] I. Grabec and S. Mikac, Plasma Phys. **16**, 1155 (1974).
[16] J. Krása, R. M. Perkin, and L. Pekárek, J. Phys. D **7**, 2541 (1974).
[17] T. Braun, J. A. Lisboa, R. E. Francke, and J. A. C. Gallas, Phys. Rev. Lett. **59**, 613 (1987).
[18] C. Wilke, R. W. Leven, and H. Deutsch, Phys. Lett. A **136**, 114 (1989).
[19] B. Albrecht, H. Deutsch, R. W. Leven, and C. Wilke, Contrib. Plasma Phys. **47**, 196 (1993).
[20] K.-D. Weltmann, H. Deutsch, H. Unger, and C. Wilke, Comments Condens. Matter Phys. **33**, 73 (1993).
[21] T. Shinbrot, Adv. Phys. **44**, 73 (1995).
[22] T. Mausbach, T. Klinger, A. Piel, A. Atipo, T. Pierre, and G. Bonhomme, Phys. Lett. A **228**, 373 (1997).
[23] K. D. Weltmann, T. Klinger, and C. Wilke, Phys. Rev. E **52**, 2106 (1995).
[24] T. Pierre, G. Bonhomme, and A. Atipo, Phys. Rev. Lett. **76**, 2290 (1996).
[25] T. Dudok de Wit, A.-L. Pecquet, J.-C. Vallet, and R. Lima, Phys. Plasmas **1**, 3288 (1994).
[26] P. Holmes, J. L. Lumley, and G. Berkooz, *Turbulence, Coherent Structures, Dynamical Systems and Symmetry* (Cambridge University Press, Cambdrige, 1996).
[27] In Ref. [8] it was pointed out that the entropy is invariant against modulation if the sidebands are nonresonant. The increase of the BD entropy is thus taken as a further support for the resonant sidebands.